Author(s): Rumfeldt, Jessica; Takala, Heikki; Liukkonen, Alli; Ihalainen, Janne

Title: UV-Vis Spectroscopy Reveals a Correlation Between Y263 and BV Protonation States in Bacteriophytochromes

Year: 2019

Version: Accepted version (Final draft)

Please cite the original version:

Rumfeldt, J., Takala, H., Liukkonen, A., & Ihalainen, J. (2019). UV-Vis Spectroscopy Reveals a Correlation Between Y263 and BV Protonation States in Bacteriophytochromes. Photochemistry and Photobiology, 95(4), 969-979. https://doi.org/10.1111/php.13095

UV-Vis Spectroscopy Reveals a Correlation Between Y263 and BV Protonation States in Bacteriophytochromes

Jessica A. Rumfeldt[1], Heikki Takala[1,2], Alli Liukkonen[1] and Janne A. Ihalainen,[1,*]

[1]University of Jyväskylä, Nanoscience Center, Department of Biological and Environmental Science, Jyväskylä, Finland

[2]University of Helsinki, Faculty of Medicine, Anatomy, Helsinki, Finland

*Corresponding author e-mail: janne.ihalainen@jyu.fi (Janne A. Ihalainen)

ABSTRACT

Red-light photosensory proteins, phytochromes, link light activation to biological functions by interconverting between two conformational states. For this, they undergo large-scale secondary and tertiary changes which follow small-scale Z to E bond photoisomerization of the covalently bound bilin chromophore. The complex network of amino acid interactions in the chromophore binding pocket plays a central role in this process. Highly conserved Y263 and H290 have been found to be important for the photoconversion yield, while H260 has been identified as important for bilin protonation and proton transfer steps. Here we focus on the roles these amino acids are playing in preserving the chemical properties of bilin in the resting Pr state of the photosensory unit of a bacteriophytochrome from *Deinococcus radiodurans*. By using pH dependent UV-Vis spectroscopy and spectral decomposition modeling, we confirm the importance of H260 for biliverdin protonation. Further, we demonstrate that in the canonical bacteriophytochromes, the pK_a value of the phenol group of the Y263 is uncommonly low. This directly influences the protonation of the bilin molecule and likely the functional properties of the protein. Our study expands the understanding of the tight interplay between the nearby amino acids and bilin in the phytochrome family.

INTRODUCTION

Phytochromes are proteins found in plants and microorganisms that function to detect and respond to the quality of light in the environment. Light absorption is due to the covalently bound bilin chromophore located in a pocket of the GAF domain (cGMP phosphor- diesterase/adenyl cyclase/FhlA). In canonical phytochromes, the GAF domain is preceded by an N-terminal PAS (Per/ARNT/Sim) domain which, together with GAF, form the chromophore-binding domain (CBD). A long helical spine connects the CBD to the phytochrome-associated PHY domain to form the photosensory module (PSM); additional long-range contacts are also made from PHY to GAF via a highly conserved PHY hairpin extension, often referred to as a "tongue". Downstream from the photosensory core is the C-terminal output region which, in the bacteriophytochromes, is typically a histidine kinase. Photoactivation initiates a phosphorelay system controlling such processes as seed germination and shade avoidance in plants and circadian rhythm and phototaxis in bacteria (1-4).

Phytochromes were first discovered in plants, and their role in all aspects of plant growth and development has been recognized over decades (2,5). The subsequent discovery of microbial phytochromes has been beneficial for all phytochrome research as their ease of purification has allowed for the determination of numerous crystal structures and a wide range of optical spectroscopy and NMR studies (6-8). Common to most phytochrome species is the covalently bound bilin chromophore, although the type of bilin conjugation is dependent on the specific subfamily: plant phytochromes bind phytochromobilin (PΦB), bacteriophytochromes (BphPs) and fungi incorporate biliverdin IXα (BV) while some cyanobacteriochromes (CBCRs), including Cph1 from *Synechocystis* sp. PCC 6803 and RcaE from *Fremyella diplosiphon,* use phycocyanobilin (PCB) (9).

Phytochrome activity is toggled on and off by switching between two conformational states: Pr and Pfr, named for their red and far-red absorbing properties, respectively (6). In Pr, bilin is in a *ZZZssa* conformation (Pr^{ZZZ}) which isomerizes to a *ZZEssa* conformation (Pfr^{ZZE}) after light absorption (Figure 1). This double bond isomerization occurs on a picosecond time scale initiating a cascade of conformational changes that are amplified throughout the protein within milliseconds, resulting in the formation of the Pfr state (10-13). Reversion to the resting Pr state can occur by a slow spontaneous thermal process called dark reversion, or by a fast, far-red light-induced interconversion. For the so-called bathy phytochromes, the Pfr is the resting state and the thermal reversion occurs from Pr to Pfr state (14). Several studies indicate that during photoconversion from Pr to Pfr, bilin undergoes a transient proton exchange (15,16), although it is not yet clear if this is an obligatory step common to all phytochromes (17).

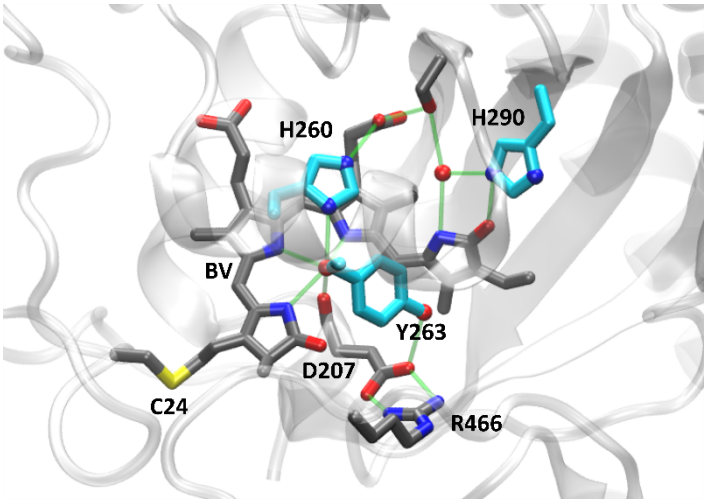

Figure 1. The chromophore binding pocket of *Dr*-PSM in the Pr state. The amino acids studied in this paper are coloured cyan while other neighbouring amino acids as well as BV in ZZZssa conformation are coloured dark grey, two ordered waters are shown as red spheres. Several key H-bond interactions (green lines) are shown including those from pyrrole water to the pyrrole nitrogens of BV, the Nδ of H260 and the backbone carbonyl of D207 and between the carboxylic

66 acid group of D207 and the guanidinium group of R466 from the tongue. Figure prepared using
67 PDB 4q0j (18) and VMD (19)

68

69 The specific chemical, spectroscopic and photoisomerization properties needed for activity are due
70 to the network of interactions formed by the highly conserved amino acids that surround the bilin
71 in the chromophore binding pocket (17,20,21). For example, when bilin is bound to the native
72 protein, all four pyrrole nitrogens are protonated in Pr^{ZZZ} and Pfr^{ZZE} resulting in a net positive
73 charge (22-24). In solution, on the other hand, bilin has a pK_a of 5.7 and PCB covalently bonded
74 to denatured phytochrome has a pK_a of 6.6 (25,26) with deprotonation likely occurring from the
75 C-ring pyrrole nitrogen (26). Of particular importance is the conserved histidine (H260 in
76 *Deinococcus radiodurans*, *Dr*) which sits in the plane on the alpha face (as defined in Rockwell et
77 al.(27)) near pyrrole rings A, B and C (Figure 1). This amino acid along with D207 on the beta
78 face, were shown to be critical for maintaining bilin protonation using site directed mutants of
79 Agp1 from *Agrobacterium fabrum* (28) and in quantum chemical calculations using PΦB as a
80 model (29). They were also shown to be involved in proton release and reuptake during
81 photoconversion of Agp1 (28). In the binding pocket, H290 (Figure 1) has also been shown to
82 influence BV protonation in Agp2, and both histidine residues have been shown to exist in their
83 neutral and positively charged protonation states with pK_a values near 7 (14,30). All these
84 protonation states may contribute to heterogeneity of the ground state with consequences for
85 complex excited state kinetics (31).

86 In this study, the different protonation states of BV and the nearby amino acids within the
87 phytochrome binding pocket of the BphP from *Dr* are studied. Specifically, the *Dr*-PSM construct
88 in the resting Pr state was monitored by UV-Vis spectroscopy in a pH range of 6.5 - 10. These pH-

titrations indicate the wild-type (WT) construct has a bilin pK_a > 10 which decreases by more than two pH units when H260 is replaced with alanine (H260A mutant). The H290T mutation on the other hand has no observable effect on the protonation state of the BV. The Y263F mutation highlights the influence of the Y263 hydroxyl on the BV protonation and absorbance with evidence for deprotonation of the phenol hydroxyl at pH values as low as 8. Comparing pK_a values from other phytochromes, the protonation state and the role of these binding site residues appears to have some species variation, but in all cases play an important role in maintaining bilin protonation. This further indicates how protein cofactors may influence the properties of the amino acid side chains in their vicinity.

MATERIALS AND METHODS

Cloning, protein expression and purification: The WT *Dr*-PSM fragment (amino acids 1–502) of *D. radiodurans* phytochrome and its Y263F and H290T variants are described elsewhere(32-34) The H260A and H260A/Y263F mutations were introduced to *Dr*-PSM with QuikChange Lightning Multi Site-Directed Mutagenesis Kit (Agilent Technologies) and primers 5'–ACC TCG CCC ATG GCC ATG CAG TAC CTG CGG AAC –3' (H260A underlined) and 5'–ACC TCG CCC ATG GCC ATG CAG TTC CTG CGG AAC ATG – 3' (H260A/Y263F underlined). Proteins were expressed and purified as previously outlined (35,36). Purified proteins from the final size-exclusion chromatography step were concentrated in 30 mM Tris pH 8 to 20–40 mg/ml, flash-frozen, and stored at -80 °C. The samples were thawed and filtered with 0.22 -μm centrifugal filter units (Amicon Ultrafree, Millipore) immediately before experimental characterization.

UV-Vis Spectroscopy: The UV-Vis measurements were carried out using a Perkin-Elmer Lambda 850 UV-vis spectrometer. The stock solutions of the phytochromes in the dark state were diluted into solutions buffered between pH 6 and 11: Mes buffer was used for pH 6 to 7.1, Tris for pH 7.2 to 9.2 and glycine for pH 9.3 to 11. The final concentration of buffer was 30 mM with constant ionic strength maintained at all pH values using NaCl. The final concentrations of *Dr*-PSM constructs were ~ 2 μM giving an absorbance at 700 nm of about 0.25 at pH 7.

Data processing and analysis: Component analysis was carried out using a 32-bit version of SPECTRALAB software (37). Before analysis, UV-Vis spectra were normalized using the absorbance at 280 nm. Scattering in the UV region was occasionally observed in solutions above pH 10 and required baseline subtraction with a first or second order polynomial. This was done in order to normalize spectra using the absorption at 280 nm. Components were made using data between 450 and 800 nm. For all constructs, the spectra measured at the lowest pH value (between pH 6.5 to 7.1) was taken as the first component Comp1. For WT, Y263F and H290T, the second component Comp2 was made by subtracting (Comp1 × fraction) from the spectra at ~ pH 10.8, then, smoothing it to make a single peak centered ~620 nm. For H260A/Y263F, Comp2 was made by subtracting (Comp1 × fraction) from the spectra at pH 8, then, smoothing it to make a single peak centered ~620 nm. For H260A, Comp2 is the spectra measured at ~ pH 10.5. The third component Comp3 required for H260A was made by subtracting (Comp1 × fraction1) and (Comp2 x fraction2) from the spectrum at ~ pH 8.5 then smoothing the resultant trace. These major components (Comp1 & Comp2 for WT, Y263F, H290T, H260A/Y263F and Comp1, Comp2 & Comp3 for H260A) were able to reconstruct the measured spectra at all pH values with a square correlation coefficient of 0.98 or greater. The use of a minor residual component (made using the

132 trace with the lowest square correlation coefficient) enabled a square correlation coefficient of
133 greater than 0.999 to be obtained for spectra at all pH values.

134 Either the absorption at 700 nm or the component contribution obtained from component
135 analysis was plotted as a function of pH and fit to equations describing titration of one or more
136 ionizable protons outlined in detail in Supporting Information (25,38).

137 Equation 1, described in detail in Supporting Information as Equation S16, was used to globally
138 fit components to the four-state equation.

139 $$S = \sum_{i=1}^{n} F_i \, [S_i(fi)] \qquad \text{Equation 1}$$

140 Briefly, i is one of four protonated species AA, AB, BA and BB outlined in the four-state cyclic
141 model below, F is a scaling factor that sets how much each species contributes to the signal being
142 fit, S is the component contribution signal associated with each of the four species and f is the
143 fraction of species i in solution which depends on pH and pK_a values. During fitting, pK_a and S_i
144 values were shared across all data sets, while F was allowed to vary between data sets and pK_{a1}
145 was defined as pK_{a2} + pK_{a3} - pK_{a4} to maintain the thermodynamic cycle. For WT and H290T the F
146 value for each species: $F_{AA}, F_{AB}, F_{BA}, F_{BB}$ was fixed to 1, 1, 0, 0 respectively, for Comp1 and 0, 0.1,
147 1, 1 respectively, for Comp2. For H260A, $F_{AA}, F_{AB}, F_{BA}, F_{BB}$ was fixed to 1, 1, 0, 0 respectively,
148 for Comp1 and 0, 0, 0.5, 1 respectively, for Comp2 and 0, 0, 1, 0 respectively, for Comp3. For
149 Y263F and H260A/Y263F, F-values are not needed as the spectral components are fitted according
150 to Eq S6a. This, because for a two-state model each species contributes 100% for respective
151 component.

152 **RESULTS**

UV-Vis absorption of pH titrations in the Pr state

The UV-Vis absorption spectra of *Dr*-PSM WT, H260A, Y263F, H260A/Y263F and H290T in the dark Pr state were measured in a range of pH buffered solutions (Figure 2, Supporting Information Figure S1). The absorption spectra of all variants have Q and Soret bands characteristic of canonical phytochromes. At low pH (7 and below), the Q band absorbance has a maximum between 702 to 696 nm, with a 1 nm red shift of Y263F and a 3, 5 and 5 nm blue shift of H290T, H260A and H260A/Y263F, respectively, relative to WT (Supporting Information, Table S1). The H260A and H260A/Y263F spectra are slightly broader than the WT spectra (Figure 2). Furthermore, the absorption coefficient is lower in the H260A samples. Using the relative intensity of UV and 700 nm absorbance after urea denaturation, using the urea denatured WT as standard, it was confirmed that this effect is not due to lower incorporation of the bound BV molecules. However, presently we do not have a solid explanation for this effect and this observation is left for further studies.

As pH increases, the intensity centered at ~700 nm decreases with concomitant increase in absorbance at ~600 nm. The pH-induced absorption changes are 100% reversible up to pH 9.8 and 85% to 95% reversible at pH 10.4.(Supporting Information Figure S2) Similar absorption changes have been observed with green/red CBCRs, where this type of shift occurs as a result of deprotonation of PCB (25). Furthermore, Escobar et al. and other groups have also described a similar effect for canonical bacteriophytochrome proteins (15,28,30) and a bathy bacteriophytochrome (39). In addition, there is no evidence for pH-induced isomerization of BV to the Pfr^{ZZE} conformation as evidenced by urea denaturation experiments.(Supporting Information, Figure S3) Therefore, we interpret the spectral changes described above as indicators of the increased population of neutral BV (BV-H_3) at high pH. Most likely, it is the ring B/C

nitrogen that becomes deprotonated (29). The spectra of the *Dr*-PSM constructs at the highest pH differed more significantly from each other than at the lowest pH. All mutants have an increased absorbance in the 600 nm region at high pH relative to WT (Figure 2) and thus larger neutral BV-H_3 populations.

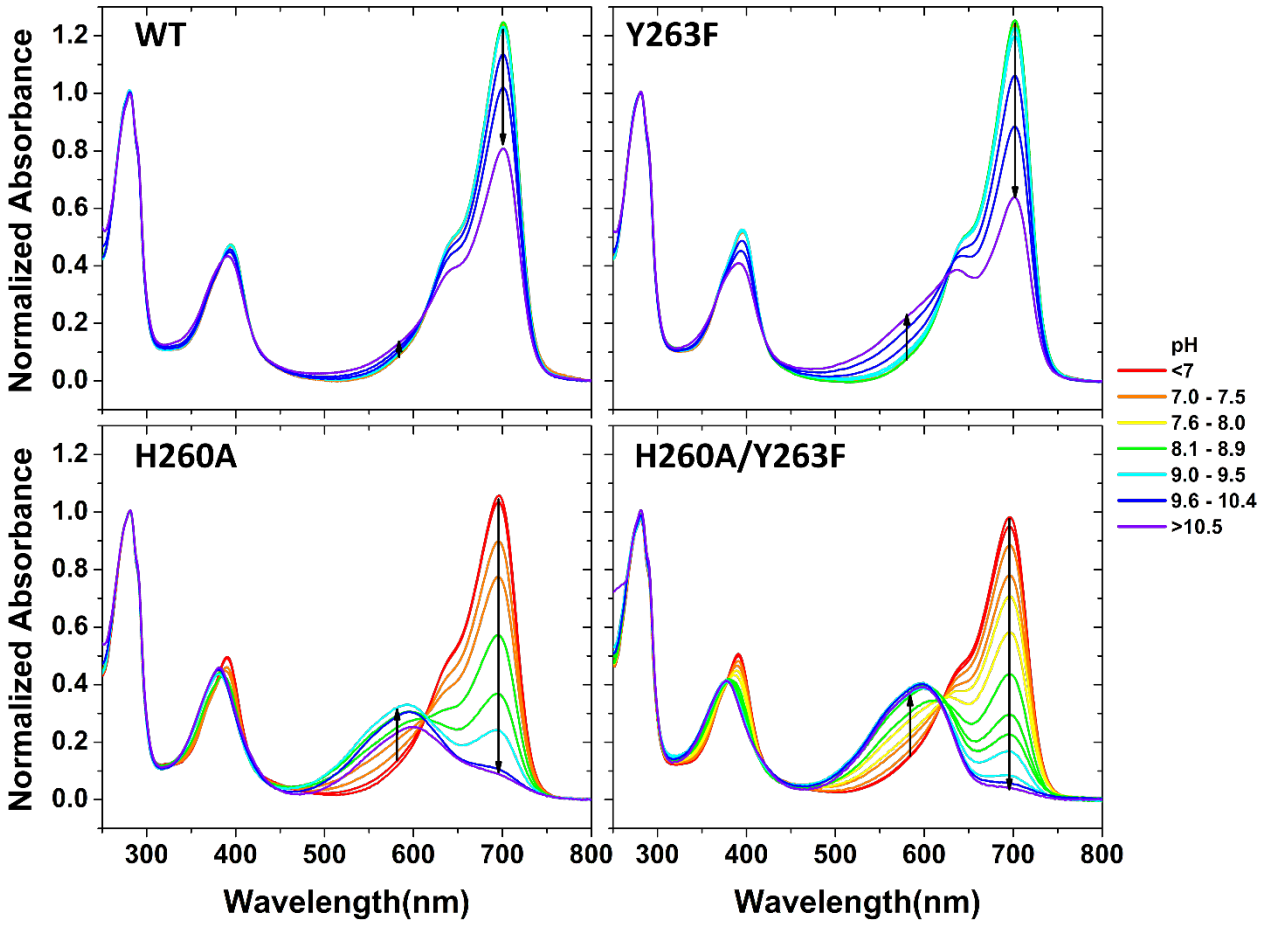

Figure 2. UV-Vis spectra of WT and mutants in the Pr state in a range of pH buffered solutions. The pH is indicated by colour: red 6-6.9, orange 7-7.5, yellow 7.6-8, green 8.1-8.9, cyan 9-9.5, blue 9.6-10.4, purple greater than 10.5. Arrows indicate the decrease/increase in absorbance at 700/600 nm as pH increases.

In order to describe the pK_a values for each construct under study, the absorbance at 700 nm was plotted versus pH. Since aggregation prevented measurement of the full transition for some constructs, the Hill equation was initially used in order to have an unbiased assessment of the cooperativity of the transition.(Table 1, Supporting Information Figure S4). Despite the high midpoints of WT, H290T and Y263F, all variants could be fit to the Hill equation. With the exception of H260A, all had Hill coefficients above 0.9 and could be fit with a two-state model assuming equilibrium between a protonated and non-protonated species with a single pK_a (Table 1, Supporting Information, Figure S4). With a Hill coefficient of 0.7, H260A was instead fit to a three-state model involving two pK_as (Table 1, Supporting Information, Figure S4).

Analysis of the absorbance at a single wavelength indicates the H260A mutation (alone or together with Y263F) significantly shifts the midpoint of the transition from greater than pH 10 to pH 8. On the other hand, single wavelength plots do not indicate any significant effect on the pH dependence of *Dr*-PSM for Y263F or H290T mutations in comparison with the WT sample (Table 1, Supporting Information, Figure S4). For this, component analysis is required which takes into account the whole Q-band absorption spectrum.

Table 1. Parameters determined from fitting absorption at 700 nm versus of pH of *Dr*-PSM variants in Pr

Protein	Hill Equation		1 or 2 pK_a model	
CBD-PHY	Hill Coef	midpoint	pK_a(1st)	pK_a(2nd)
WT	1.1 ± 0.03	10.8 ± 0.1	10.9 ± 0.1	
Y263F	1.1 ± 0.02	10.7 ± 0.1	10.6 ± 0.1	
H260A	0.7 ± 0.02	8.0 ± 0.02	7.7 ± 0.05	8.9 ± 0.11
H260A/Y263F	0.9 ± 0.03	8.0 ± 0.02	8.1 ± 0.02	
H290T	1.0 ± 0.1	10.9 ± 0.1	10.9 ± 0.1	

Errors are the 95% confidence interval

Component analysis

Hill coefficients less than 1 in pH titrations (specifically observed for H260A) suggest that the deprotonation process of the biliverdin deviates from two-state behaviour. To investigate this further, component analysis was carried out on all variants using the UV-Vis spectra between 450 and 800 nm. With the exception of H260A, pH titration spectra can be sufficiently reconstructed with two major components: one with a peak centered at ~700 nm called component one (Comp1), the other with a peak centered at ~620 nm called component two (Comp2) shown in Figure 3 and in Supporting Information Figure S1 for H290T. A minor residual component is also needed that accounts for small shifts in wavelength maximum as a function of pH. For H260A, an additional major component (Comp3) is required to reconstruct the spectra between 450 and 800 nm as a function of pH shown in green (Figure 3).

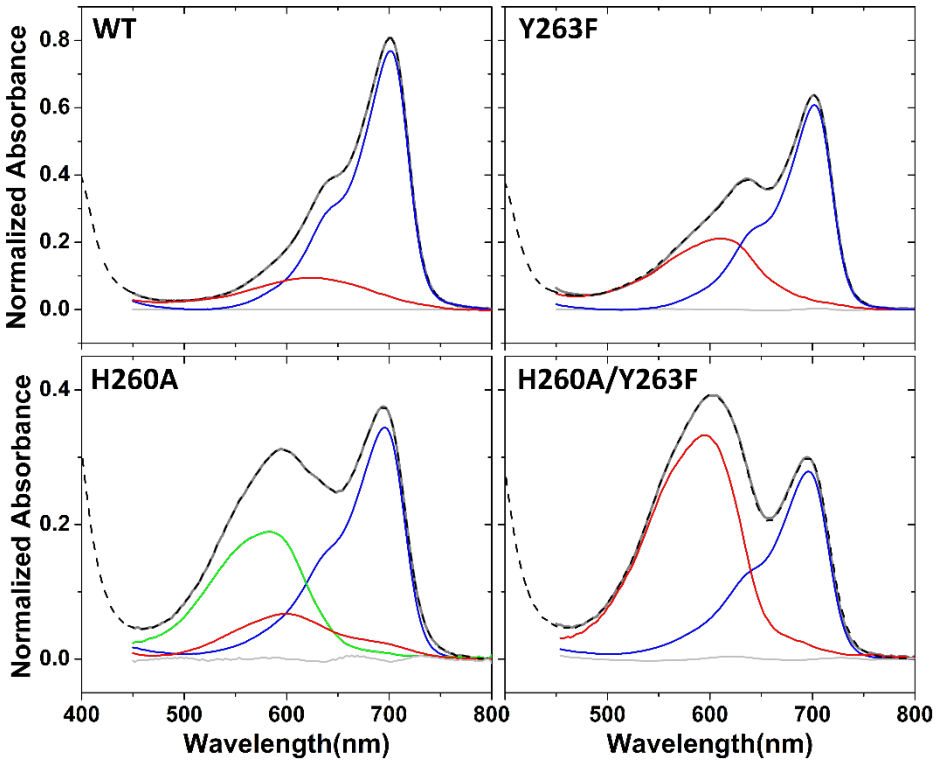

Figure 3. Spectral decomposition. UV-Vis spectra of the Pr state at pH 10.8 for WT and Y263F and pH 8.5 for H260A and H260A/Y263F (dashed lines) are shown decomposed into components.

For WT, Y263F, H260A/Y263F and H290T (shown in Supporting Information) two major components Comp1 and Comp2 (blue and red solid lines respectively) and a minor component (light grey line) are needed to reconstruct the spectra between 450 and 800 nm at all pHs. For H260A, an additional component Comp3 is needed (green line). The sum of components are shown as a solid grey line.

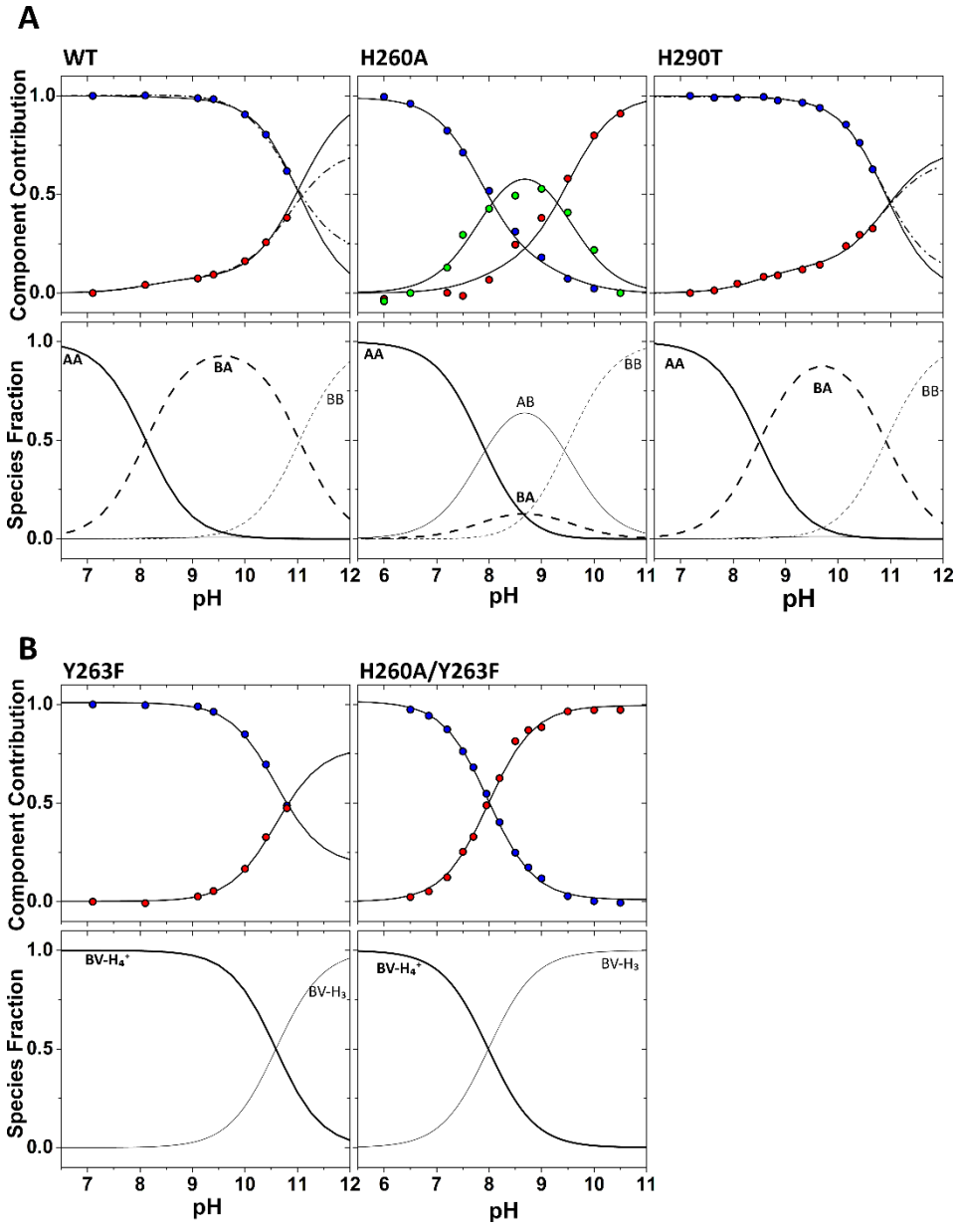

Figure 4. Global fitting of major spectral components. A) WT, H260A and H290F B) Y263F and H260A/Y263F Top row: The contribution of Comp1 (blue circles), Comp2 (red circles) and Comp3 (green circles) to the absorption spectra are plotted as a function of pH. Solid lines represent the global fit using the model with four pK_as in A and one pK_a in B. The dash-dot-lines represents a fit with two pK_as for WT and H290T. Bottom row: the fraction of different protonated species as a function of pH calculated from the fitting parameters. In A these are AA (corresponding to BV-H_4^+/Y263-OH, thick solid line); BA (corresponding to BV-H_4^+/Y263-O^-, thick dashed line); AB (corresponding BV-H_3/Y263-OH, thin solid line) and BB (corresponding, BV-H_3/Y263-O^-, thin dashed line). These line types match those used to outline each of the four species in Figure 5. In B the two protonation states are BV-H_4^+ (thick solid line) and BV-H_3 (thin solid line).

For each construct, the contribution of each major component was plotted as a function of pH and globally fit to models involving one to four pK_a values (Figures 4 and 5, Table 2, Supporting Information Table S2). The fitting resulted in convergence for all data sets despite the high midpoints of WT, H290T and Y263F. In order to compare fitting to data at 700 nm, a single fit of Comp1 to one pK_a was also carried out where possible (Table 1, Supporting Information, Table 2). For WT and H290T, there is a small amplitude change before the major transition begins at pH 9.5 – most clearly observed for Comp2 – resulting in deviation when the data is fit to a model with one pK_a (Figure 4, Supporting Information, Figure S5). The deviation in this region is also observed when the titration is performed using Hepes and Bicine buffer as well as with a *Dr*-PSM monomer construct ruling out changes in dimerization or buffer effects as a source of the asymmetry.(Supporting Information, Figure S5) A better fit is achieved when a model involving two pK_as is used: the small amplitude change corresponding to a pK_a ~8.5 and the large amplitude

change corresponding to pK_a ~10.8 (Figure 4, Table 2). Comp1 alone does not show these two phases as clearly and can be reasonably fit with one pK_a similar to data at 700 nm, demonstrating the motivation and advantage of using component analysis and global fitting (Table1, 2, Supporting Information, Table 2).

Importantly, unlike WT and H290T, constructs with the Y263 mutation, namely Y263F and H260A/Y263F, involve only one pK_a.(Figure 4) This is observed for both single fits to Comp1 and global fits of Comp1 and Comp2 together (Table 2, Supporting Information, Table S2). This confirms that a single species is being titrated in Y263F and H260A/Y263F constructs, and their respective pK_a values of 10.6 and 8.0 reflect the deprotonation of BV as follows:

$$(BV\text{-}H_4)^+ \leftrightarrow (BV\text{-}H_3) + H^+ \qquad \text{Equation 2}$$

Table 2. Parameters from global fits using a four-pK_a model for constructs with Y263, and one-pK_a model for constructs with F263.

Protein	Spectral	BV		Y263-OH	
Dr-PSM	components[a]	pK_{a1}	pK_{a2}	pK_{a3}	pK_{a4}
WT	C1&C2	10.3	11.0	8.4*	9.1
H290T	C1&C2	10.0*	10.8	8.4	9.2
H260A	C1&C2&C3	7.9	8.7	8.7	9.5
Y263F[b]	C1&C2	10.3*	-	-	-
H260A/Y263F[b]	C1&C2	8.0	-	-	-

[a] C1, C2, C3 are the components Comp1, Comp2 and Comp3 used to deconvolute the spectra
The pK_a values 1 to 4 correspond the model in Figure 5. Standard errors from Origin fitting ranged from 0.3 to 4 % of the fitted value. The pK_a values reported in the table are an average from fits to two separate titrations. The 95% confidence interval was in general 0.2 pH units except values with asterisks,(*) which had 95% confidence intervals between 0.4 and 0.6 pH units.
[b] For Y263F and H260A/Y263F, the data can only reasonably be fit (single or global) with one pK_a.

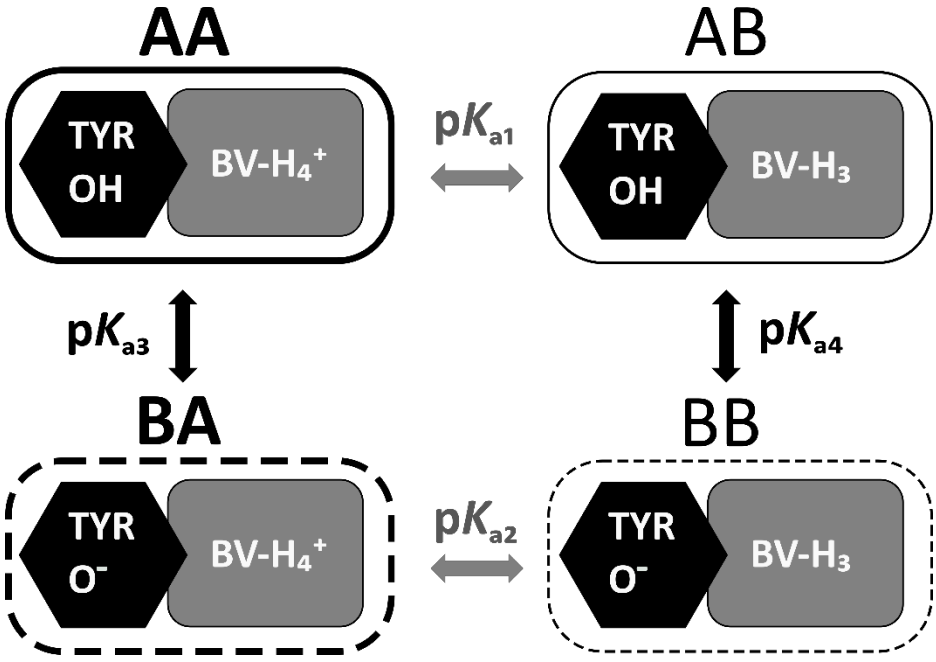

Figure 5. The four-state cyclic model with reciprocal influence of BV and Y263-OH titrations. In this model, the chromophore binding pocket of *Dr*-PSM can exist in four different protonation states designated as species AA, BA, AB and BB. In AA and BA (thick lines), BV is fully protonated and positively charged with the Y263 hydroxyl protonated or deprotonated, respectively. In AB and BB (thin lines), BV is neutral with Y263 hydroxyl protonated or deprotonated, respectively. The pK_{a1} and pK_{a2} describe the titration of BV when Y263-OH is protonated and deprotonated, respectively. The pK_{a3} and pK_{a4} describe the titration of Y263-OH when BV is protonated and deprotonated, respectively.

Since the pH dependence of *Dr*-PSM is simplified in constructs where the Y263 hydroxyl group (Y263-OH) is removed, this group is a likely source of the asymmetry and complexity observed in pH titrations of WT, H290T and H260A. The nearby negative charge of Y263-O^- can influence the absorption properties of BV and make it appear similar to the deprotonated form, which is compensated for by the increased contribution of Comp2 in spectral decomposition. This hypothesis was tested further by measuring the UV-Vis absorbance of the tyrosine band at 280 nm

as well as fluorescence emission at 340 nm.(See Supporting Information Figure S7, S8, S9) Since the aim is to detect the deprotonation of a single tyrosine out of eleven, observing the spectral changes is challenging; However, the results of both experimental methods are consistent with Y263-OH deprotonation. For WT and H290T, the large amplitude change with pK_a ~10.7 is therefore considered to be from titration of BV while the small amplitude change with pK_a ~8.4 is assigned to the titration of Y263-OH. The complexity attributed to the Y263-OH group in WT and H290T is even more pronounced in *Dr*-PSM with the H260A mutation. As discussed above, H260A requires three major spectral components (Comp1, Comp2, Comp3) to reconstruct the spectra while only two (Comp1, Comp2) are necessary for H260A/Y263F (Figure 3). The pH dependence of Comp3 in H260A (green circles in Figure 4), shows a rise and fall in population of an intermediate indicating at least two pK_as; however, a sequential three-state model fails to fully describe the data (Supporting Information, Figure S6). The four-state cyclic model was instead considered which includes deprotonation of both BV and Y263-OH (Figure 5). In this model, four different protonation states can be defined for *Dr*-PSM: AA (BV-H_4^+/Y263-OH), BA (BV-H_4^+/Y263-O^-), AB (BV-H_3/Y263-OH), BB (BV-H_3/Y263-O^-), and their relative population changes with pH. Since initial attempts at fitting the components of H260A separately required at least two pK_as (not shown), each component likely reflects a combination of absorption spectra arising from at least two of these protonation states. When fitting the data to the four-state model, it was therefore assumed that Comp1 accounts for the fraction of species AA and BA in solution, Comp2 the fraction of species AB and BB in solution and Comp3 the fraction of species AB in solution. With these assumptions, the four-state model provides a good global fit of the three major components of H260A (Figure 4).

Fitting the data of H260A gives two pK_as for BV deprotonation, one when the tyrosine hydroxyl is protonated Y263-OH (pK_{a1} = 7.9) and the other when it is deprotonated Y263-O^- (pK_{a2} = 8.7). It also gives two pK_as for Y263-OH deprotonation, one when BV is positively charged (pK_{a3} = 8.7) and the other when BV is neutral (pK_{a4} = 9.5). Using the results of the fit, the fraction of each of the four *Dr*-PSM protonation states: AA, BA, AB and BB can be plotted as a function of pH (Figure 4A, bottom row). With this in mind, the WT and H290T data were also globally fit to the four-state model (Figure 4, Table 2). Since the model is underdetermined by the data (i.e. there are only two components and the full titration cannot be observed) the fitted pK_a values have a certain degree of error which has been estimated in Supporting Information Figure S10; nevertheless, the pK_{a3} and pK_{a4} values describing the titration of Y263-OH are very similar for WT, H290T and H260A, ~8.4 and 9.4, respectively (Table 2). For WT and H290T, the pK_{a2} of ~11 for BV in the presence of Y263-O^- predicts that BV deprotonation is only fully complete at ~pH 12. The pK_{a3} of ~8.4 means that the Y263 hydroxyl is ~20% deprotonated at pH 8 and fully deprotonated at pH 9.5 (Figure 4).

Contributions of each spectral component to the UV-Vis spectra of *Dr*-PSM

A UV-Vis spectrum at a given pH is a combination of the individual spectra of the different protonated species in solution. For WT, H290T and H260A these species are assumed to be AA, BA, AB and BB, outlined in Figure 5. For Y263F and H260A/Y263F, which have a single pK_a value, there are two species: BV-H_4^+ and BV-H_3 as outlined in Equation 2. From the fractional population of species as a function of pH shown in Figure 4, the fully protonated state, AA (BV-H_4^+ for the Y263F mutants), is well isolated (>99% populated) at pH values less than 8.5 for Y263F and pH values lower than pH 6 for the other constructs. Since protein aggregation was usually noticeable near pH 6, Comp1 was taken from spectra measured between pH 6.5 and 7.1 and

therefore, for all but Y263F, may have some contribution from deprotonated species. The fully deprotonated species (BB or BV-H_3) can be observed at pH values > 10 in titrations of H260A/Y263F, while for WT, H290T and Y263F, the fully deprotonated species is only significantly populated at pH values greater than 11, which is out of range of the protein stability and therefore unable to be measured by UV-Vis. Even for H260A, the spectrum at pH 10.5 may contain some contribution from BA and AB in addition to the major species BB.

The presence of intermediate protonated species is most obvious in titrations of H260A which requires a third major component, Comp3. From Figure 4, the fraction of species AB is much higher than BA between pH 8 and 9. In this case, Comp3, made from subtracting a fraction of Comp1 from the spectrum measured at pH ~7.2, is likely very similar to the spectrum of isolated AB but may also have contributions from BA (Figure 4). For WT and H290T, the species BA is well isolated at pH ~9.5. This suggests that the spectrum of BA is very similar to that of AA with slightly more absorbance around 600 nm. This is reasonable given the only difference is the protonation state of Y263.

DISCUSSION

In this study, bilin protonation of *Dr*-PSM was monitored by UV-Vis absorption spectroscopy of WT and mutants in the dark Pr conformation. Absorption spectra of all *Dr*-PSM constructs have so-called Q and Soret bands characteristic of canonical phytochromes (Figure 2). All constructs were photoactive and photoreversible (data not shown). This indicates phytochromes with mutations are properly folded and functional.

pH dependent absorption spectra of *Dr*-PSM: deprotonation in the chromophore binding site

Deprotonation of the bilin B/C nitrogen typically results in a decrease in absorbance at 700 nm and an increase at 600 nm (ref (15) and references therein). This is clearly observed in plots of absorption at 700 nm versus pH for all constructs and is interpreted as a result of BV deprotonation as in Equation 2 (Supporting Information, Figure S4). For WT, Y263F and H290T, absorbance at 700 nm does not significantly decrease until ~ pH 9, indicating the chromophore is fully protonated up to this point. In contrast, pH titrations of H260A and H260A/Y263F show that absorption at 700 nm is close to the minimum at pH 9, and each have midpoints of ~ pH 8 (Table 1, Supporting Information, Figure S4). This is in line with Resonance Raman of H260A of full length *Dr*-BphP at pH 8 which shows approximately half of the intensity of the N-H in-plane mode of the wild-type indicating the bilin is approximately half deprotonated (34). These data demonstrate the key role H260 plays in maintaining BV protonation.

Although the single and double mutants have similar midpoints, their Hill coefficients reveal differences in titration behaviour. For H260A/Y263F, the coefficient of 0.9 indicates a single deprotonation of BV as in Equation 2, while for H260A, the coefficient of 0.7 suggests an additional ionization is taking place. The most evident ionization group is Y263-OH, initially considered since this hydroxyl is absent in the double mutant. Firstly, the amino acid at position 263 is in close proximity to BV with observable differences in the absorption spectra attributable to this mutation; for example, at high pH, constructs containing the Y263F mutation have higher absorbance in the 600 nm region and the Soret band relative to their Y263 counterparts (Figure 2). As in the model outlined in Figure 5, the absorbance decrease resulting from pH increase observed for H260A is therefore interpreted as a reflection of both BV and Y263-OH deprotonation. Spectral

component analysis, discussed below, as well as UV absorbance and fluorescence (Supporting Information) provides further support for this model and also provides evidence for titration of Y263-OH in WT and H290T.

Spectral component analysis confirms titration of Y263 concomitant with chromophore deprotonation in WT *Dr*-PSM

For H260A, three major spectral components and a minor component are needed to deconvolute the Q band region throughout the pH range 6.5 to 10.5, while two major and one minor component are sufficient for WT, Y263F, H290T and H260A/Y263F (Figure 3, Supporting Information Figure S1). For all constructs, Comp1 is the spectrum measured at pH 6.5 to 7 taken to represent the protonated form, whereas Comp2 and Comp3 (required only for H260A), have peaks between ~585 nm and ~620 nm that resemble a deprotonated species. The constructs without the Y263-OH group, Y263F and H260A/Y263F, have simple sigmoidal transitions: Comp1 and Comp2 can be globally fit using a single pK_a attributed to BV deprotonation (Figure 4, Table 2, and Supporting Information Figure S5). For WT and the other two mutants that have the Y263-OH group, component analysis indicates that along with BV deprotonation, an additional pH dependent event is taking place. In particular for H260A, Comp1 and Comp2 have clear inflection points, and Comp3 increases and decreases in a way typical of intermediate formation. In this case, a global fit is best carried out using the four-state model outlined in Figure 5 which takes into account deprotonation of BV and Y263-OH (Figure 4, Table 2). For WT and H290T, deprotonation of Y263-OH is manifested in the small amplitude changes of Comp2 at ~ pH 8-9. Global fitting of these constructs requires at least two pK_a values (Figure 4, Supporting Information Table S2, Figure S5), but data can also be fit using the four pK_a model outlined in Figure 5.(Figure 4) These fits give two pK_a values for bilin deprotonation: pK_{a1} and pK_{a2} when the Y263 hydroxyl is

393 protonated and deprotonated respectively, and two pK_a values for Y263 hydroxyl deprotonation:
394 pK_{a3} and pK_{a4} when bilin is protonated and deprotonated, respectively (Table 2).

395 The pK_a values for BV in Table 2 are reasonable given the wide range of values found in
396 other phytochrome species, discussed further below. On the other hand, the pK_{a3} value of ~8.5
397 determined for the Y263 containing constructs WT, H290T and H260A is much lower than the
398 average pK_a value of 10.3 found for tyrosine in proteins (40). Such a low tyrosine pK_a can be found
399 for example in UDP-galactose 4-epimerase (41). In this protein, Y149 has a very low pK_a of 6.08
400 attributed to the positive electrostatic field created by nicotinamide adenine dinucleotide and a
401 lysine. Similarly, in glutathione transferase A1-1, active site Y9 has a pK_a of 8.1 which, when
402 nearby R15 is mutated to alanine, increases to 8.8 due to removal of the positive charge (42). In
403 *Dr*-PSM, the chromophore binding pocket is shielded from solvent by the tongue so that a
404 positively charged BV could also be lowering the pK_{a3} of Y263-OH. Indeed, the pK_{a4} for Y263-
405 OH in the presence of the neutral BV is ~9.4 for all Y263 containing constructs, closer to a typical
406 tyrosine value.

407 Our spectral component analysis therefore detected a deprotonation event in Y263-OH in
408 WT and H290T, which is not readily apparent in single wavelength plots. For H260A, multiple
409 ionization events are apparent in single wavelength plots in the form of a low Hill coefficient;
410 however, component analysis confirmed the existence of intermediate ionization states within the
411 chromophore binding site and allowed for the development of a detailed model of BV and Y263-
412 OH deprotonation.

413 **Comparison of bilin pK_a with other phytochrome species – role of bilin protonation**

414 Although the type and amount of domains that make up phytochromes is species dependent, the
415 binding site architecture is in general similar enough that it is worth comparing the binding

chemical properties in order to better understand how amino acid arrangement effects the binding site properties. The high bilin pK_a value found for *Dr*-PSM is consistent with the pK_a value of 11.1 found for Agp1, which is also a canonical BV containing BphP (28). The cyanobacterial Cph1 and RcaE have bilin pK_a values of 9.0 and 5.6, respectively (15,25,30). A pK_a value greater than 9.5 indicates that the bilin is in the cationic form under physiological conditions which may be important for activation; for example, it was suggested that the deprotonated chromophore can only be weakly excited (15,29) and is less likely to photoisomerize (29). For RcaE, the low pK_a of the Pr state is responsible for the photochromicity of the protein: the deprotonated chromophore in ZZZ conformation has green absorbance, which, after photoisomerization to the ZZE conformation, results in a protonated red absorbing chromophore due to an increase of the pK_a (25).

In the bathy phytochrome Agp2, the Pfr^{ZZE} resting state deprotonates at the B/C nitrogen with an apparent pK_a of 7.6 (14). This relatively low pK_a does not occur with a change in the overall net charge of the molecule, instead, deprotonation of ring B/C is concomitant with keto/enol isomerization of ring D. The location of the resulting positive charge distribution is influenced by the protonation state of H278 (H290 in *Dr*-BphP) which in turn influences the dark reversion rate of the Pfr state. These studies together suggest there is large degree of species variation in bilin pK_a values with the bilin protonation state serving different functions such as photoactivation, photochromicity and dark reversion.

Residues in the chromophore binding pocket: H260, H290 and Y263

The amino acids in the chromophore binding pocket form interactions with bilin that produce its specific functional chemistry and geometry. According to structural studies, the conserved H260

H-bonds to the C-ring propionate of bilin through its Nε group while its Nδ group interacts with the pyrrole (Figure 1). The so-called pyrrole water in turn H-bonds with the imidazole nitrogens of rings A, B and C, maintaining their protonation. This and other studies confirm that removal of this histidine typically results in a significant population of the neutral bilin species at physiological pH values. For example, constructs with the H260A mutation in this study result in an ~2.3 unit decrease to pK_a values near 8 (Table 2). This near identical decrease in the pK_{a1} and pK_{a2} values of WT or the single pK_a value of Y263F, indicates the effect of the mutation is the same regardless of the protonation state or presence of the Y263 hydroxyl. A 2.3 unit decrease in pK_a was also seen in the dark Pr^{ZZZ} state of Agp1 as replacement of this histidine with alanine changed the value from 11.1 to 8.8 (28). In the bathy phytochrome Agp2, replacement of H260 not only decreases bilin protonation but also partially inverses the direction of dark reversion from Pfr to Pr (28,34,39). Interestingly, the bilin pK_a of 5.6 in RcaE is similar to the value obtained in denaturing conditions and is attributed to a leucine at the corresponding H260 position. When this leucine is replaced with a histidine, the pK_a increases 2 units in the green absorbing state (Pg^{ZZZ}) but decreases in the red absorbing state (Pr^{ZZE}).

In Cph1, this histidine may have a slightly different function. Substitution with glutamic acid has no observable effect on the pK_a of Pr^{ZZZ} but rather selectively decreases the pK_a of Pfr^{ZZE} (30). In this case, the H260 itself was observed to undergo deprotonation in the Pr state with a pK_a of 7.5 accompanied by a decrease in Q band absorbance. This equilibrium between the cationic H260 and the one singly protonated at Nε is a natural origin of the heterogeneity in the Pr^{ZZZ} state of Cph1 (30,43,44), also observed in complex excited-state dynamics (31). There is, however, no evidence for H260 deprotonation in this pH range in *Dr*-PSM; for example, in Y263F there is no change in contribution of Comp1 or Comp2 until after pH 9 (Figure 4) (28).

462 Another histidine in the binding pocket, H290, makes up an important interaction network
463 among the BV D-ring and water molecules that affects bilin conformation and photoconversion
464 (33,45). When bilin is in the Pr^{ZZZ} conformation, it H-bonds through its Nδ to both an ordered
465 water and the D ring carbonyl maintaining the 44° out of plane rotation of ring-D relative to B and
466 C (34,46). After photoisomerization, H-bonding switches from the D ring in Pr^{ZZZ} to the C-ring
467 propionate in Pfr^{ZZE}. Studies with *Rp*-BphP3, where this conserved interaction with H290 is
468 augmented with H-bonds from Ser and Lys side chains (47,48), and *Sa*P1, where it is absent due
469 to a natural Thr replacement (45), indicated the amount of hydrogen bonding between the D-ring
470 and the amino acids correlates with the excited-state lifetime of bilin and the extent of non-
471 productive decay back to Pr. On the other hand, comparison of the IR-absorption band of the D-
472 ring carbonyl between WT, the H290T mutation in *Dr*-PSM, and SaP1, led to the conclusion that
473 the D-ring carbonyl actually has stronger H-bonding, but to the water molecules present in the
474 absence of the histidne (33). This also influences the excited state decay processes of the biliverdin.
475 As mentioned above, in bathy Agp2, the neutral form of this histidine stabilizes a tautomer
476 of bilin that has a decreased rate of dark reversion back to Pfr. The cationic histidine is thought to
477 deprotonate with a pK_a of 6.7 (14). In our study, pH titrations of WT and H290T appear very
478 similar to each other with similar pK_a values and no evidence for a change in protonation state of
479 H290 was observed (Table 2, Figure 4). Therefore, this histidine can influence the quantum
480 efficiency of Pfr photoconversion in canonical phytochromes and – in a pH dependent manner –
481 dark reversion in bathy phytochromes, but does not appear to have an effect on bilin protonation.
482 Another key amino acid involved in the bilin H-bonding network is the highly conserved
483 Y263. Not only does it form important H-bonds to bilin in both Pr^{ZZZ} and Pfr^{ZZE}, but it is also one
484 of several amino acids that make up the hydrophobic pocket surrounding ring D (34). It was also

found to influence photoconversion quantum efficiency (49). In the Pr conformation, Y263 has the potential to H-bond with the carboxylate of D207 (46) and has been proposed to play a role in keeping the tongue rigidly fixed to the GAF domain through its involvement in the conserved interaction between D207 and R466 (36,50). Recently it was found that the Y263F mutation resulted in the uncoupling of structural changes in *Dr*-PSM, enabling the tongue to adopt a Pfr-like □-helix fold while the chromophore remains in the ZZZ conformation of the Pr state (32).

In this study, the Y263F mutation on its own does not seem to influence BV protonation in *Dr*-PSM which was also the case in Cph1 (49). Although removal of the OH group does not have an effect in and of itself, its protonation state does affect the pK_a of BV: the deprotonated negative form stabilizes the positive charge of BV resulting in two observed pK_a values. In the alternative scenario, the Y263H mutation in Cph1 introduces a positive charge in the binding-pocket resulting in partial deprotonation of the chromophore (49). In this study, stabilization of BV protonation by the phenolate group is not readily affected by other changes in *Dr*-PSM as the pKa_2 is ~0.8 pH units higher than pKa_1 for all three Y263-containing isoforms (Table 2).

Summary

The protonation properties of BV and binding-pocket amino acids in *Dr*-PSM were monitored by UV-Vis spectrometry. Our study indicates a direct influence of the nearby amino acids on the absorption properties, and moreover on the protonation properties of the BV. The pH induced changes in spectra were analyzed by component analysis which enabled detection of more than one deprotonation event. The large amplitude decrease in the 700 nm was mainly attributed to BV deprotonation while the increase ~ 600 nm was attributed to a combination of BV and Y263-OH deprotonation. These simultaneous titrations result in four pK_a values, two for BV and two for tyrosine. The high BV p*K*a values for WT and Y263F were decreased by two units when H260

was replaced with alanine. The other histidine in the binding pocket, H290, showed little to no change in pK_a. Although highly conserved, comparison of the properties of binding-pocket residues suggest their function may be somewhat different depending on the PHY species. We show that about 20% of WT has a deprotonated Y263 under biological conditions at pH 7.8. This observation may explain the source of heterogeneity of the Pr state, observed in several phytochrome species (31,51,52). There may be aspects of the low pK_a of Y263 that are important for phytochrome function, for example, in regards to the proposed proton transfer reaction during photoisomerization (48), which then may influence the isomerization yield of the chromophore. Further, the Y263 tyrosinate may quench BV fluorescence differently than tyrosine, and as such, our results may help further the design of the phytochrome-based fluorescent proteins.(53,54)

ACKNOWLEDGMENTS*:* The research was supported by the Academy of Finland grants 285461 (H.T.), and 296135, Jane and Erkko foundation, and the Magnus Ehrnrooth foundation (J.A.I). We would like to thank Heikki Häkkänen for assistance with UV-Vis absorption spectroscopy.

SUPPORTING INFORMATION

Figure S1. UV-Vis spectra as a function of pH and spectral decomposition for H290T.

Figure S2. Reversibility of BV absorbance

Figure S3. Maintenance of the Pr^{ZZZ} conformation of BV in high pH as indicated by Urea denaturation.

Figure S4. Plot of absorption at 700 nm as a function of pH for WT, H290T, H260A, Y263F and H260A/Y263F.

Figure S5. Deviation observed from a fit to one pK_a for WT and H290T but not for Y263F or H260A/Y263F.

Figure S6. Global fitting of the major spectral components of H260A to the sequential 3-state model.

Figure 7. Changes in UV-absorption as a function of pH

Figure 8. Plots of the absorption difference at the specific wavelength regions indicated by arrows in Figure 7.

Figure 9. UV Fluorescence

Figure 10. Error estimation

Table S1. Wavelength maxima determined from UV-Vis spectra of *Dr*-PSM variants in Pr

Table S2. Parameters determined from fitting spectral components to models involving one to two pK_a values

Supporting Methods: Models used for fitting pH titration data

ABBREVIATIONS

CBD, chromophore-binding domain; PSM, photosensory module which includes PAS, GAF and PHY domains; *Dr, Deinococcus radiodurans*; *Dr*-PSM, photosensory module from *Deinococcus radiodurans*; BphP, bacteriophytochrome; BV, biliverdin Ixα; BV-H_3, neutral BV with three of four pyrrole nitrogens protonated; BV-H_4^+, positively charged BV with all four pyrrole nitrogens protonated; Pr, the red-light absorbing state of the phytochrome molecule; Pfr, the far- red-light

548 absorbing state of the phytochrome molecule; Pr^{ZZZ}, the bilin chromphore in the Pr state
549 conformation ZZZ; Pr^{ZZE}, the bilin chromophore in the Pfr state conformation ZZE; WT, wild-
550 type; Comp1, component one; Comp2, component two; Comp3, component three; AA, the
551 protonation state of *Dr*-PSM with BV-H_4^+ and Y263-OH; AB, the protonation state of *Dr*-PSM
552 with BV-H_3 and Y263-O^-; BA, the protonation state of *Dr*-PSM with BV-H_4^+ and Y263-O^-; AA,
553 the protonation state of *Dr*-PSM with BV-H_3 and Y263-O^-;

554 **REFERENCES**

555 1. Auldridge, M. E. and K. T. Forest. (2011) Bacterial phytochromes: More than meets the light.
556 *Crit. Rev. Biochem. Mol. Biol.* **46**, 67-88.

557 2. Wang, H. and H. Wang. (2015) Phytochrome signaling: Time to tighten up the loose ends.
558 *Mol. Plant.* **8**, 540-551.

559 3. Gross, R., and D, B. (2012) Two-Component Systems in Bacteria, in Caister Academic Press,
560 Pool, UK.

561 4. Fiedler, B., T. Borner and A. Wilde. (2005) Phototaxis in the cyanobacterium synechocystis
562 sp. PCC 6803: Role of different photoreceptors. *Photochem. Photobiol.* **81**, 1481-1488.

563 5. Butler, W. L., K. H. Norris, H. W. Siegelman and S. B. Hendricks. (1959) Detection, assay,
564 and preliminary purification of the pigment controlling photoresponsive development of plants.
565 *Proc. Natl. Acad. Sci. U. S. A.* **45**, 1703-1708.

566 6. Ulijasz, A. T. and R. D. Vierstra. (2011) Phytochrome structure and photochemistry: Recent
567 advances toward a complete molecular picture. *Curr. Opin. Plant Biol.* **14**, 498-506.

568 7. Rockwell, N. C. and J. C. Lagarias. (2017) Phytochrome diversification in cyanobacteria and
569 eukaryotic algae. *Curr. Opin. Plant Biol.* **37**, 87-93.

570 8. Nagatani, A. (2010) Phytochrome: Structural basis for its functions. *Curr. Opin. Plant Biol.*
571 **13**, 565-570.

572 9. Rockwell, N. C., Y. Su and J. C. Lagarias. (2006) Phytochrome structure and signaling
573 mechanisms. *Annual Review of Plant Biology* **57**, 837-858.

574 10. Bjorling, A., O. Berntsson, H. Lehtivuori, H. Takala, A. J. Hughes, M. Panman, M. Hoernke,
575 S. Niebling, L. Henry, R. Henning, I. Kosheleva, V. Chukharev, N. V. Tkachenko, A. Menzel,
576 G. Newby, D. Khakhulin, M. Wulff, J. A. Ihalainen and S. Westenhoff. (2016) Structural
577 photoactivation of a full-length bacterial phytochrome. *Science advances* **2**, e1600920-e1600920.

578 11. Mroginski, M. A., D. H. Murgida and P. Hildebrandt. (2007) The chromophore structural
579 changes during the photocycle of phytochrome: A combined resonance raman and quantum
580 chemical approach. *Acc. Chem. Res.* **40**, 258-266.

581 12. Yang, Y., M. Linke, T. von Haimberger, J. Hahn, R. Matute, L. Gonzalez, P. Schmieder and
582 K. Heyne. (2012) Real-time tracking of phytochrome's orientational changes during pr
583 photoisomerization. *J. Am. Chem. Soc.* **134**, 1408-1411.

584 13. Ihalainen, J. A., E. Gustavsson, L. Schroeder, S. Donnini, H. Lehtivuori, L. Isaksson, C.
585 Thoing, V. Modi, O. Berntsson, B. Stucki-Buchli, A. Liukkonen, H. Hakkanen, E. Kalenius, S.

586 Westenhoff and T. Kottke. (2018) Chromophore-protein interplay during the phytochrome
587 photocycle revealed by step-scan FTIR spectroscopy. *J. Am. Chem. Soc.* **140**, 12396-12404.

588 14. Escobar, F. V., P. Piwowarski, J. Salewski, N. Michael, M. F. Lopez, A. Rupp, B. M.
589 Qureshi, P. Scheerer, F. Bartl, N. Frankenberg-Dinkel, F. Siebert, M. A. Mroginski and P.
590 Hildebrandt. (2015) A protonation-coupled feedback mechanism controls the signalling process
591 in bathy phytochromes. *Nature chemistry* **7**, 423-430.

592 15. van Thor, J. J., B. Borucki, W. Crielaard, H. Otto, T. Lamparter, J. Hughes, K. J. Hellingwerf
593 and M. P. Heyn. (2001) Light-induced proton release and proton uptake reactions in the
594 cyanobacterial phytochrome Cph1. *Biochemistry (N. Y.)* **40**, 11460-11471.

595 16. Borucki, B., D. v. Stetten, S. Seibeck, T. Lamparter, N. Michael, M. A. Mroginski, H. Otto,
596 D. H. Murgida, M. P. Heyn and P. Hildebrandt. (2005) Light-induced proton release of
597 phytochrome is coupled to the transient deprotonation of the tetrapyrrole chromophore. *J. Biol.*
598 *Chem.* **280**, 34358-34364.

599 17. Borucki, B. (2006) Proton transfer in the photoreceptors phytochrome and photoactive
600 yellow protein. *Photochemical & photobiological sciences : Official journal of the European*
601 *Photochemistry Association and the European Society for Photobiology* **5**, 553-556.

602 18. Burgie, E. S., T. Wang, A. N. Bussell, J. M. Walker, H. Li and R. D. Vierstra. (2014)
603 Crystallographic and electron microscopic analyses of a bacterial phytochrome reveal local and
604 global rearrangements during photoconversion. *J. Biol. Chem.* **289**, 24573-24587.

19. Humphrey, W., A. Dalke and K. Schulten. (1996) VMD: Visual molecular dynamics. *J. Mol. Graph.* **14**, 33-8, 27-8.

20. Rohmer, T., C. Lang, W. Gartner, J. Hughes and J. Matysik. (2010) Role of the protein cavity in phytochrome chromoprotein assembly and double-bond isomerization: A comparison with model compounds. *Photochem. Photobiol.* **86**, 856-861.

21. Karniol, B., J. R. Wagner, J. M. Walker and R. D. Vierstra. (2005) Phylogenetic analysis of the phytochrome superfamily reveals distinct microbial subfamilies of photoreceptors. *Biochem. J.* **392**, 103-116.

22. Song, C., T. Rohmer, M. Tiersch, J. Zaanen, J. Hughes and J. Matysik. (2013) Solid-state NMR spectroscopy to probe photoactivation in canonical phytochromes. *Photochem. Photobiol.* **89**, 259-273.

23. Andel, F.,3rd, J. T. Murphy, J. A. Haas, M. T. McDowell, I. van der Hoef, J. Lugtenburg, J. C. Lagarias and R. A. Mathies. (2000) Probing the photoreaction mechanism of phytochrome through analysis of resonance raman vibrational spectra of recombinant analogues. *Biochemistry* **39**, 2667-2676.

24. Schwinte, P., W. Gärtner, S. Sharda, M. Mroginski, P. Hildebrandt and F. Siebert. (2009) The photoreactions of recombinant phytochrome CphA from the cyanobacterium calothrix PCC7601: A low-temperature UV-vis and FTIR study. *Photochem. Photobiol.* **85**, 239-249.

25. Hirose, Y., N. C. Rockwell, K. Nishiyama, R. Narikawa, Y. Ukaji, K. Inomata, J. C. Lagarias and M. Ikeuchi. (2013) Green/red cyanobacteriochromes regulate complementary chromatic acclimation via a protochromic photocycle. *Proc. Natl. Acad. Sci. U. S. A.* **110**, 4974-4979.

26. Shang, L., N. C. Rockwell, S. S. Martin and J. C. Lagarias. (2010) Biliverdin amides reveal roles for propionate side chains in bilin reductase recognition and in holophytochrome assembly and photoconversion. *Biochemistry (N. Y.)* **49**, 6070.

27. Rockwell, N. C., L. Shang, S. S. Martin and J. C. Lagarias. (2009) Distinct classes of red/far-red photochemistry within the phytochrome superfamily. *Proc. Natl. Acad. Sci. U. S. A.* **106**, 6123-6127.

28. von Stetten, D., S. Seibeck, N. Michael, P. Scheerer, M. A. Mroginski, D. H. Murigida, N. Krauss, M. P. Heyn, P. Hildebrandt, B. Borucki and T. Lamparter. (2007) Highly conserved residues asp-197 and his-250 in Agp1 phytochrome control the proton affinity of the chromophore and pfr formation. *J. Biol. Chem.* **282**, 2116-2123.

29. Borg, A. and B. Durbeej. (2008) Which factors determine the acidity of the phytochromobilin chromophore of plant phytochrome? *Phys. Chem. Chem. Phys.* **10**, 2528-2537.

30. Escobar, F. V., C. Lang, A. Takiden, C. Schneider, J. Balke, J. Hughes, U. Alexiev, P. Hildebrandt and M. A. Mroginski. (2017) Protonation-dependent structural heterogeneity in the chromophore binding site of cyanobacterial phytochrome Cph1. *J Phys Chem B* **121**, 47-57.

31. Kirpich, J. S., L. T. Mix, S. S. Martin, N. C. Rockwell, J. C. Lagarias and D. S. Larsen. (2018) Protonation heterogeneity modulates the ultrafast photocycle initiation dynamics of phytochrome Cph1. *J. Phys. Chem. Lett.* **9**, 3454-3462.

32. Takala, H., H. Lehtivuori, O. Berntsson, A. Hughes, R. Nanekar, S. Niebling, M. Panman, L. Henry, A. Menzel, S. Westenhoff and J. A. Ihalainen. (2018) On the (un)coupling of the chromophore, tongue interactions and overall conformation in a bacterial phytochrome. *J. Biol. Chem.*

33. Lenngren, N., P. Edlund, H. Takala, B. Stucki-Buchli, J. Rumfeldt, I. Peshev, H. Hakkanen, S. Westenhoff and J. A. Ihalainen. (2018) Coordination of the biliverdin D-ring in bacteriophytochromes. *Phys. Chem. Chem. Phys.* **20**, 18216-18225.

34. Wagner, J. R., J. Zhang, D. v. Stetten, M. Gunther, D. H. Murgida, M. A. Mroginski, J. M. Walker, K. T. Forest, P. Hildebrandt and R. D. Vierstra. (2008) Mutational analysis of deinococcus radiodurans bacteriophytochrome reveals key amino acids necessary for the photochromicity and proton exchange cycle of phytochromes. *The Journal of biological chemistry* **283**, 12212-12226.

35. Lehtivuori, H., I. Rissanen, H. Takala, J. Bamford, N. V. Tkachenko and J. A. Ihalainen. (2013) Fluorescence properties of the chromophore-binding domain of bacteriophytochrome from deinococcus radiodurans. *J Phys Chem B* **117**, 11049-11057.

36. Takala, H., A. Bjorling, O. Berntsson, H. Lehtivuori, S. Niebling, M. Hoernke, I. Kosheleva, R. Henning, A. Menzel, J. A. Ihalainen and S. Westenhoff. (2014) Signal amplification and transduction in phytochrome photosensors. *Nature* **509**, 245-248.

662 37. Davydov, D. R., E. Deprez, G. H. Hoa, T. V. Knyushko, G. P. Kuznetsova, Y. M. Koen and
663 A. I. Archakov. (1995) High-pressure-induced transitions in microsomal cytochrome P450 2B4
664 in solution: Evidence for conformational inhomogeneity in the oligomers. *Arch. Biochem.*
665 *Biophys.* **320**, 330-344.

666 38. Nielsen, J. E. (2009) Chapter 9 Analyzing Enzymatic pH Activity Profiles and Protein
667 Titration Curves using Structure-Based pKa Calculations and Titration Curve Fitting, in pp 233-
668 258, Elesvier Inc, .

669 39. Zienicke, B., I. Molina, R. Glenz, P. Singer, D. Ehmer, F. V. Escobar, P. Hildebrandt, R.
670 Diller and T. Lamparter. (2013) Unusual spectral properties of bacteriophytochrome Agp2 result
671 from a deprotonation of the chromophore in the red-absorbing form pr. *The Journal of biological*
672 *chemistry* **288**, 31738-31751.

673 40. Grimsley, G. R., J. M. Scholtz and C. N. Pace. (2009) A summary of the measured pK values
674 of the ionizable groups in folded proteins. *Protein Sci.* **18**, 247-251.

675 41. Liu, Y., J. B. Thoden, J. Kim, E. Berger, A. M. Gulick, F. J. Ruzicka, H. M. Holden and P.
676 A. Frey. (1997) Mechanistic roles of tyrosine 149 and serine 124 in UDP-galactose 4-epimerase
677 from escherichia coli. *Biochemistry (N. Y.)* **36**, 10675-10684.

678 42. Bjornestedt, R., G. Stenberg, M. Widersten, P. G. Board, I. Sinning, T. A. Jones and B.
679 Mannervik. (1995) Functional significance of arginine 15 in the active site of human class alpha
680 glutathione transferase A1-1. *J. Mol. Biol.* **247**, 765-773.

681 43. Song, C., G. Psakis, C. Lang, J. Mailliet, W. Gartner, J. Hughes and J. Matysik. (2011) Two
682 ground state isoforms and a chromophore D-ring photoflip triggering extensive intramolecular
683 changes in a canonical phytochrome. *Proc. Natl. Acad. Sci. U. S. A.* **108**, 3842-3847.

684 44. Dasgupta, J., R. R. Frontiera, K. C. Taylor, J. C. Lagarias and R. A. Mathies. (2009) Ultrafast
685 excited-state isomerization in phytochrome revealed by femtosecond stimulated raman
686 spectroscopy. *Proc. Natl. Acad. Sci. U. S. A.* **106**, 1784-1789.

687 45. Mathes, T., J. Ravensbergen, M. Kloz, T. Gleichmann, K. D. Gallagher, N. C. Woitowich, R.
688 St Peter, S. E. Kovaleva, E. A. Stojkovic and J. T. Kennis. (2015) Femto- to microsecond
689 photodynamics of an unusual bacteriophytochrome. *J. Phys. Chem. Lett.* **6**, 239-243.

690 46. Wagner, J. R., J. Zhang, J. S. Brunzelle, R. D. Vierstra and K. T. Forest. (2007) High
691 resolution structure of deinococcus bacteriophytochrome yields new insights into phytochrome
692 architecture and evolution. *J. Biol. Chem.* **282**, 12298-12309.

693 47. Toh, K. C., E. A. Stojkovic, I. H. van Stokkum, K. Moffat and J. T. Kennis. (2011)
694 Fluorescence quantum yield and photochemistry of bacteriophytochrome constructs. *Phys.*
695 *Chem. Chem. Phys.* **13**, 11985-11997.

696 48. Toh, K. C., E. A. Stojkovic, I. H. van Stokkum, K. Moffat and J. T. Kennis. (2010) Proton-
697 transfer and hydrogen-bond interactions determine fluorescence quantum yield and
698 photochemical efficiency of bacteriophytochrome. *Proc. Natl. Acad. Sci. U. S. A.* **107**, 9170-
699 9175.

49. Mailliet, J., G. Psakis, K. Feilke, V. Sineshchekov, L. O. Essen and J. Hughes. (2011) Spectroscopy and a high-resolution crystal structure of Tyr263 mutants of cyanobacterial phytochrome Cph1. *J. Mol. Biol.* **413**, 115-127.

50. Song, C., M. A. Mroginski, C. Lang, J. Kopycki, W. Gartner, J. Matysik and J. Hughes. (2018) 3D structures of plant phytochrome A as pr and pfr from solid-state NMR: Implications for molecular function. *Front. Plant. Sci.* **9**, 498.

51. Kim, P. W., N. C. Rockwell, S. S. Martin, J. C. Lagarias and D. S. Larsen. (2014) Dynamic inhomogeneity in the photodynamics of cyanobacterial phytochrome Cph1. *Biochemistry* **53**, 2818-2826.

52. Heyne, K., J. Herbst, D. Stehlik, B. Esteban, T. Lamparter, J. Hughes and R. Diller. (2002) Ultrafast dynamics of phytochrome from the cyanobacterium synechocystis, reconstituted with phycocyanobilin and phycoerythrobilin. *Biophys. J.* **82**, 1004-1016.

53. Bhattacharya, S., M. E. Auldridge, H. Lehtivuori, J. A. Ihalainen and K. T. Forest. (2014) Origins of fluorescence in evolved bacteriophytochromes. *J. Biol. Chem.* **289**, 32144-32152.

54. Chernov, K. G., T. A. Redchuk, E. S. Omelina and V. V. Verkhusha. (2017) Near-infrared fluorescent proteins, biosensors, and optogenetic tools engineered from phytochromes. *Chem. Rev.* **117**, 6423-6446.

FIGURE CAPTIONS

Figure 1. The chromophore binding pocket of *Dr*-PSM in the Pr state. The amino acids studied in this paper are coloured cyan while other neighbouring amino acids as well as BV in ZZZssa conformation are coloured dark grey, two ordered waters are shown as red spheres. Several key H-bond interactions (green lines) are shown including those from pyrrole water to the pyrrole nitrogens of BV, the Nδ of H260 and the backbone carbonyl of D207 and between the carboxylic acid group of D207 and the guanidinium group of R466 from the tongue. Figure prepared using PDB 4q0j (18) and VMD (19)

Figure 2. UV-Vis spectra of WT and mutants in the Pr state in a range of pH buffered solutions. The pH is indicated by colour: red 6-6.9, orange 7-7.5, yellow 7.6-8, green 8.1-8.9, cyan 9-9.5, blue 9.6-10.4, purple greater than 10.5. Arrows indicate the decrease/increase in absorbance at 700/600 nm as pH increases.

Figure 3. Spectral decomposition. UV-Vis spectra of the Pr state at pH 10.8 for WT and Y263F and pH 8.5 for H260A and H260A/Y263F (dashed lines) are shown decomposed into components. For WT, Y263F, H260A/Y263F and H290T (shown in Supporting Information) two major components Comp1 and Comp2 (blue and red solid lines respectively) and a minor component (light grey line) are needed to reconstruct the spectra between 450 and 800 nm at all pHs. For H260A, an additional component Comp3 is needed (green line). The sum of components are shown as a solid grey line.

Figure 4. Global fitting of major spectral components. A) WT, H260A and H290F B) Y263F and H260A/Y263F Top row: The contribution of Comp1 (blue circles), Comp2 (red circles) and Comp3 (green circles) to the absorption spectra are plotted as a function of pH. Solid lines

represent the global fit using the model with four pK_as in A and one pK_a in B. The dash-dot-lines represents a fit with two pK_as for WT and H290T. Bottom row: the fraction of different protonated species as a function of pH calculated from the fitting parameters. In A these are AA (corresponding to BV-H_4^+/Y263-OH, thick solid line); BA (corresponding to BV-H_4^+/Y263-O^-, thick dashed line); AB (corresponding BV-H_3/Y263-OH, thin solid line) and BB (corresponding, BV-H_3/Y263-O^-, thin dashed line). These line types match those used to outline each of the four species in Figure 5. In B the two protonation states are BV-H_4^+ (thick solid line) and BV-H_3 (thin solid line).

Figure 5. The four-state cyclic model with reciprocal influence of BV and Y263-OH titrations. In this model, the chromophore binding pocket of *Dr*-PSM can exist in four different protonation states designated as species AA, BA, AB and BB. In AA and BA (thick lines), BV is fully protonated and positively charged with the Y263 hydroxyl protonated or deprotonated, respectively. In AB and BB (thin lines), BV is neutral with Y263 hydroxyl protonated or deprotonated, respectively. The pK_{a1} and pK_{a2} describe the titration of BV when Y263-OH is protonated and deprotonated, respectively. The pK_{a3} and pK_{a4} describe the titration of Y263-OH when BV is protonated and deprotonated, respectively.